

**USING PHASE SHIFT
INTERFEROMETRY TO
MEASURE THE TOPOGRAPHY OF
THIN METAL FILMS**

By

Jonathon Zdunski

A thesis submitted in partial fulfillment of the
requirements for the degree of

Bachelor of Science

Houghton University

May 2023

Signature of Author.....

Department of Physics
May 10, 2023

.....
Dr. Brandon Hoffman
Professor of Physics
Research Supervisor

.....
Dr. Mark Yuly
Professor of Physics

USING PHASE SHIFT INTERFEROMETRY TO MEASURE THE TOPOGRAPHY OF THIN METAL FILMS

By

Jonathon Zdunski

Submitted to the Department of Physics
on May 10, 2023 in partial fulfillment of the
requirement for the degree of
Bachelor of Science

Abstract

A low-cost phase-shifting laser interferometer is being constructed at Houghton University to measure the thickness and topography of thin metal films produced with a variety of deposition parameters. The modified Twyman-Green Interferometer uses a 632 nm laser. Three piezoelectric ceramic stacks move a reference mirror up to 883 nm along the direction of the beam with a precision of <1 nm. The interference pattern is captured by a 2 MP camera. The system is suspended by springs and uses eddy current damping to decrease the movement of the system. A housing mounted to the outer frame blocks wind produced by the building's air handling system. A LabVIEW program controls the mirror movement and fits a sine function to the intensity of each pixel vs. reference mirror position. An intensity plot of the fitted phase shifts represents the topography. Initial tests using two $\lambda/10$ flat mirrors indicate that the individual pixel height measurements are repeatable within about 1.6 nm. Assuming the film surface is smooth, the maximum repeatability of the overall topography should therefore be <1 nm.

Thesis Supervisor: Dr. Brandon Hoffman
Title: Professor of Physics

TABLE OF CONTENTS

Chapter 1: Introduction.....	5
1.1. Light	5
1.1.1. Light as a Wave	5
1.1.2. Interference of Light	5
1.2. Ether.....	6
1.3. Interferometry	7
1.3.1. General Interferometer.....	7
1.3.2. Advancement in Interferometry	8
1.3.2.1. Michelson’s Experiment.....	8
1.3.2.2. Twyman–Green Interferometer	9
1.3.2.3. Modified Twyman-Green Interferometers	12
1.3.2.4. Interferometers Using Lasers.....	13
1.3.2.5. Phase Shifting Interferometer	15
1.4. Thin Metal Films.....	17
1.4.1. Introduction to Thin metal films.....	17
1.4.2. Experiments on Thin Metal Films.....	17
1.5. Houghton University Thin Metal Films Laboratory	18
1.5.1. Houghton University Laser Interferometer.....	18
1.5.2. Other Thin Metal Film experiments at Houghton University	19
Chapter 2: Theory.....	21
2.1. Introduction	21
2.2. Light and Interference.....	21
2.2.1. Single Beam of Light.....	21
2.2.2. Multiple Beams of Light.....	22
Chapter 3: Apparatus	26
3.1. Layout of the Apparatus.....	26
3.2. Mechanical Vibration Isolation	27
3.3. Collecting and Analyzing the Data.....	31
Chapter 4: Results.....	35
4.1. Topography of Mirror.....	35
4.2. Determining Timing of Tests	37
4.3. Repeatability.....	39
Chapter 5: Conclusion / Future Plans.....	41

TABLE OF FIGURES

Figure 1. Theoretical plot of the combination of the electric field of two waves.....	6
Figure 2. General model of an interferometer	7
Figure 3. Diagram of Michelson's interferometer from his experiment in 1881	8
Figure 4. Graph showing the results of Michelson's interferometer Experiment	9
Figure 5. Layout of Twyman's interferometer while testing a prism.....	11
Figure 6. Example of an output of Twyman's Experiment.....	11
Figure 7. Diagram of the design of the experiment by Steimle and Wang.....	13
Figure 8. Experimental setup from Tien, Lyu, and Jyu's experiment.....	14
Figure 9. 3-D Topography of one of the films from the Tien Experiment.....	15
Figure 10. Diagram of a general phase shift interferometer	16
Figure 11. Images from Grosso and Crane's phase shifting interferometer	17
Figure 12. Surface topography of SiO ₂ films	18
Figure 13. A simplified image of the interferometer at Houghton	23
Figure 14. Picture of the Houghton University interferometer	28
Figure 15. An image of the holder of the reference mirror	28
Figure 16. A circuit diagram of the electronics used to move the mirror	29
Figure 17. An image showing the housing and the springs.....	29
Figure 18. The Eddy Current Damping box	30
Figure 19. The section of the table that is inside the Eddy Current Damping Box.....	31
Figure 20. A flow chart of how the data being processed	32
Figure 21. Diagram showing the background subtraction done to the topography.....	34
Figure 22. Picture of an interference pattern and the area being tested	35
Figure 23. Image of a graph showing the intensity of a pixel over time from last year ..	36
Figure 24. Plot of a graph showing the intensity of a pixel over time from this year	36
Figure 25. Surface topography of the section of the mirror outlined in Figure 22	37
Figure 26. Plot of a test done that was 50 s long, with 50 total pictures.....	38
Figure 27. Plot of a test done that was 200 s long, with 200 total pictures	38
Figure 28. Plot of a test done during the day	39
Figure 29. Surface topography of tests done in quick succession of each other	40
Figure 30. Plot of the difference between the two tests shown in Figure 29	40

Chapter 1

INTRODUCTION

1.1. Light

1.1.1. Light as a Wave

For hundreds of years in the scientific community, there was an argument on whether light was a wave or a particle. In the early 1800's, Thomas Young created an experiment [1] that is now known as the double slit experiment that was able to help lead the argument for the wave nature of light.

Young set up an experiment in which light passed through two small slits in a piece of paper. The light coming out of the separate slits then acted like two independent sources of light. These sources of light then continued to a wall at the other side of the room. When the light reached the wall, the two beams of light seemed to have interfered with each other, causing a line of light that went from dark, to light, and back to dark. This pattern then repeated. This experiment showed that instead of light acting like a particle, where there would have been only two deposits of light particles, the light instead acted like a wave, where the light sources interfered with each other, depending on the distance traveled by the light. From this, it was possible to then model how different beams of light interfered with each other.

1.1.2. Interference of Light

The intensity of light is determined by the amplitudes of the electric and magnetic fields. When two or more beams of light come together, the electric and magnetic fields of the waves add as vectors. Therefore, the combined amplitudes and resulting intensity may be greater or less than those of the original beams, depending on the relative directions of the fields. This addition is considered the interference of the two beams.

An example of the interference between two waves can be seen in Figure 1. Wave 1 and Wave 2 represent the electric field of the two electromagnetic waves. When two waves combine, the result is a new electric field for a new electromagnetic wave or beam of light. It is then possible to use the electric field to determine the intensity of the electromagnetic wave or

beam of light. This is because the intensity of the wave is proportional to the electric field squared.

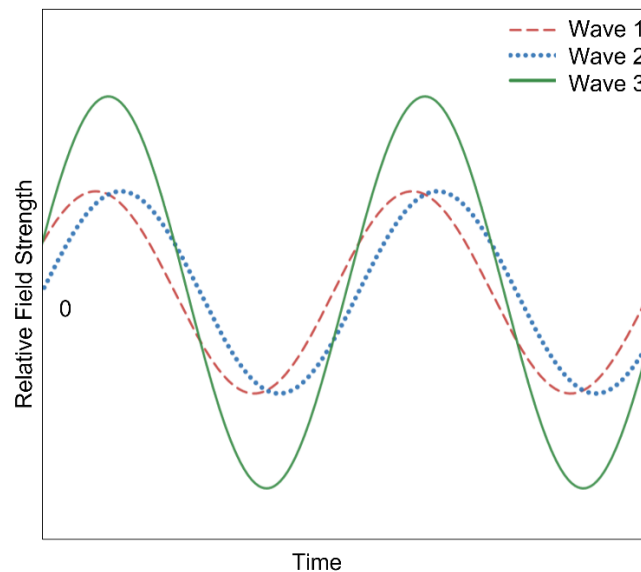


Figure 1. Theoretical plot of the combination of the electric field of two waves. Waves 1 and 2 represent the electric field of the electromagnetic waves. When Wave 1 is added to Wave 2, the result is Wave 3. The intensity of the wave or beam of light is proportional to the amplitude of the wave squared.

1.2. *Ether*

When light and other electromagnetic waves were being first studied, it was believed that light had to travel through a medium, like any other wave. The answer at the time to the “missing” medium was ether [2]. Ether was believed to be a substance that filled all space, even between atoms of different bodies. Ether was believed to have an extremely small density and to be very elastic. These properties of ether then allowed electromagnetic waves to propagate through it.

Due to ether being believed to be the medium light travels through, the existence of ether can be tested using interferometry. Interferometry is a method of measurement in physics that uses the interference of light to measure many different things, including the surface topography of materials to a precise amount. The first interferometer [3] was created by Albert A. Michelson to test the existence of ether. Ether was also believed to be stationary with all physical bodies, like the Earth, passing through it. Michelson’s experiment tested if

a stationary ether existed. The experiment used the property of interference of light to function.

1.3. Interferometry

1.3.1. General Interferometer

An interferometer uses the interference of light to determine the distance traveled by each of the beams of light. A general interferometer can be seen in Figure 2. An interferometer works by first splitting a beam of light into two different directions. The beams travel a distance that is defined by the experiment, return to the beam splitter, combine, and travel to the screen, so the researchers can see the interference of the two beams. Depending on the distance traveled by the two beams, when recombining, the beams interfere with each other in different ways. An interferometer can also be used to measure the speed of light in one medium compared to another. This is possible because as the light travels through the two mediums, and they have a different speed of light, the waves would be at two different phases after recombining. This is the premise that was used by Michelson in his interferometer.

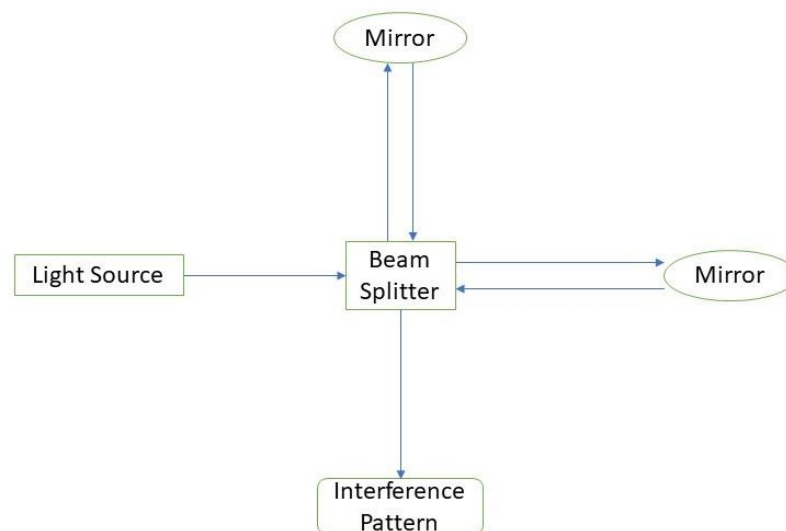


Figure 2. General model of an interferometer. A beam of light first enters the beam splitter from the Light Source. The light is then split into two separate beams, each of which travels to one of the mirrors. The beams then reflect off the mirrors and recombine at the beam splitter. The resulting interference pattern of the two beams of light is then able to be analyzed.

1.3.2. Advancement in Interferometry

1.3.2.1. Michelson's Experiment

To determine if stationary ether exists, Michelson used the experimental setup [3] shown in Figure 3. The experiment involved having one of the arms set up the direction of the Earth's movement, and the other at a 90° angle, perpendicular to the movement of the Earth. The light traveled from the source, was split by the beam splitter, and traveled down both arms. The beams of light then reflected off the mirrors and recombine at the beam splitter. The recombined beam of light is analyzed. The apparatus was then used to get data at many different times of the day, over many days. The setup was then also rotated 90° . This rotation of the apparatus continued until all orientations were tested, then the data were analyzed.

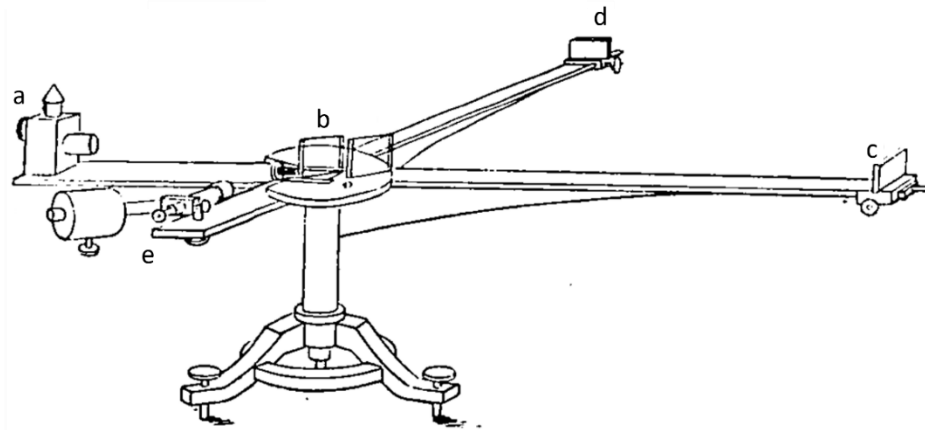


Figure 3. Diagram of Michelson's interferometer from his experiment in 1881. The light source starts at a on the left, and goes to the glass plate b. It then splits and goes to c and d, which are equal distances from b. They then combine and come back to e. Figure taken from Ref. [3].

If stationary ether existed, and the Earth was moving through the ether, the speeds of the two beams would be different. This is due to the relative motion of the ether of the two beams. The Earth moving through the stationary ether would, relative to the Earth, act like the ether is moving in the opposite direction of the Earth's movement. For any wave, including electromagnetic waves, if the medium has a velocity with a component in the direction of the wave, the wave's velocity would be different than if there was no velocity component in that direction. This is why the apparatus in the experiment was positioned with one arm parallel

to the direction of the Earth's movement and one perpendicular to the movement. Only one of the arms would be affected by the movement of the medium.

After running through all of the tests at the different times of days and different rotations, it was determined that there was not enough evidence to confirm the existence of stationary ether. The results of the experiment can be seen in Figure 4, where the dotted line was predicted data assuming stationary ether, and the solid line was the experimental data. If stationary ether existed, there was presumed to be a large difference between the two light beams. Due to there not being as much of a difference between the two beams of light, it was determined that stationary ether did not exist. Since this experiment, there have been many advancements in interferometers [4, 5, 6]. One of these advancements came in the form of the Twyman–Green interferometer [4].

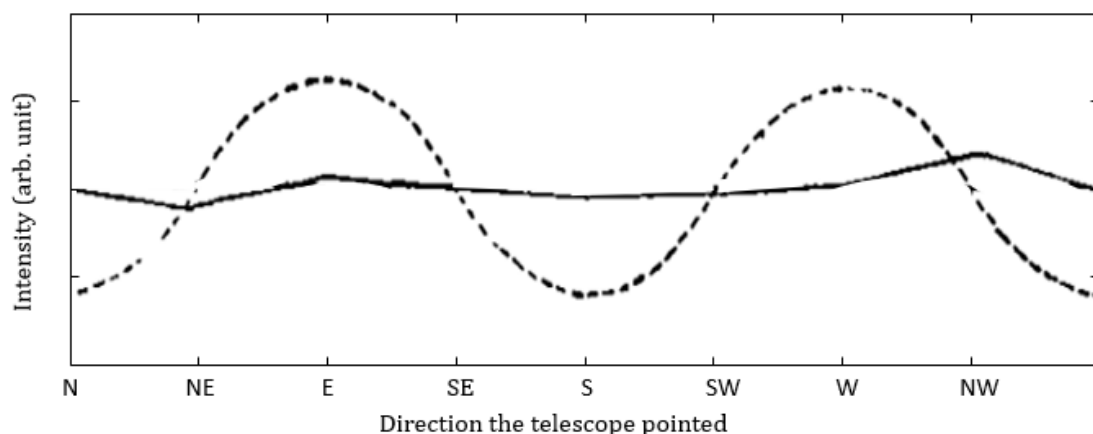


Figure 4. Graph showing the results of Michelson's interferometer Experiment. The dotted line is the predicted data if stationary ether existed. The solid line is the actual experimental data. From this data, it was determined that stationary ether did not exist. The fact that the actual data do not have the periodicity that the expected value is used to disprove stationary ether. Figure modified from Ref. [3].

1.3.2.2. Twyman–Green Interferometer

When a light beam's cross section is increased, it is possible to interpret the new wide beam as a group of smaller narrow beams with the same wave features traveling together. When two of these wide beams interfere with each other, it can be modeled as two groups of

narrow beams interfering with each other. This means that for any point on a cross section of the combined beam, the interference between the two beams is similar to Figure 1. Because each of these narrow beams acts independently, the interference at one point is not affected by another point. Using this property of the beams of light, it is possible to see the differences in the distance traveled by each point on the beam of light. One of the uses for this is to test if lenses for different objects work. This is what Twyman made his interferometer for.

In 1816, Frank Twyman and Arthur Green created a new interferometer [4] that was modeled off the Michelson interferometer [3]. This interferometer is known as the Twyman-Green interferometer. One of the main differences between the Twyman-Green interferometer and the Michelson interferometer is the size of the beam of light. In the Twyman-Green interferometer, the beam of light is collimated to a desired cross sectional area. Twyman then showed some of the modifications that could be made to the interferometer [7] to test lenses and prisms.

In 1921, Twyman used the interferometer from his discussion in an experiment [8] to test the quality of lenses and prisms. The interferometer used by Twyman in his experiment can be seen in Figure 5. The setup shown in Figure 5 was used to test the quality of the prism that is placed at E. To test the quality of a lens, the prism E and the mirror F would be replaced with the lens being tested, and a convex mirror. This mirror was placed so that the center of the mirror was at the focal length of the lens that was being tested. This caused the light that reflected off the mirror to reflect correctly back through the lens and recombine with the control beam of light.

An example of the output of Twyman's interferometer can be seen in Figure 6. The lines on the top part of the image are the interference pattern of the two beams of light that recombine in the apparatus. Twyman was able to show how his device was effective in testing the quality of lenses with a focal length of 101 mm to 686 mm. Over the years, other researchers were able to modify a Twyman-Green interferometer to test other materials as well.

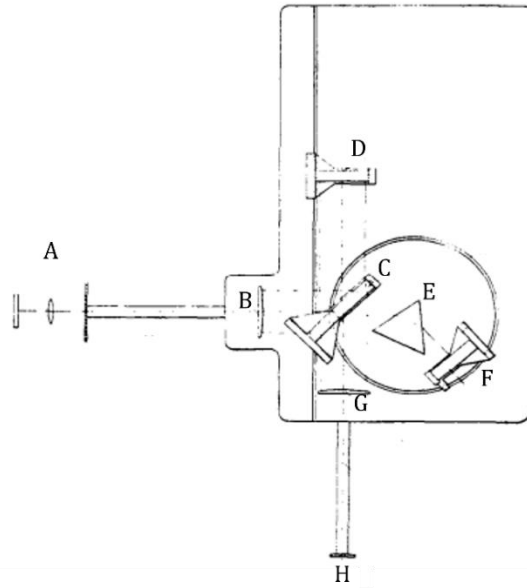


Figure 5. Layout of Twyman's interferometer while testing a prism. The beam of light starts at A, goes through a diverging lens, and travels to B, where the beam is collimated to the desired cross sectional area. The beam then travels to C, where it is split, and travels to a mirror D, and a prism E. The beam that travels through the prism E then travels to another mirror F. The two beams then reflect off the mirrors, and return to C, where they are recombined. The beam is focused on G, so the user to see the interference pattern at the desired diameter at point H. Figure taken from Ref. [8].

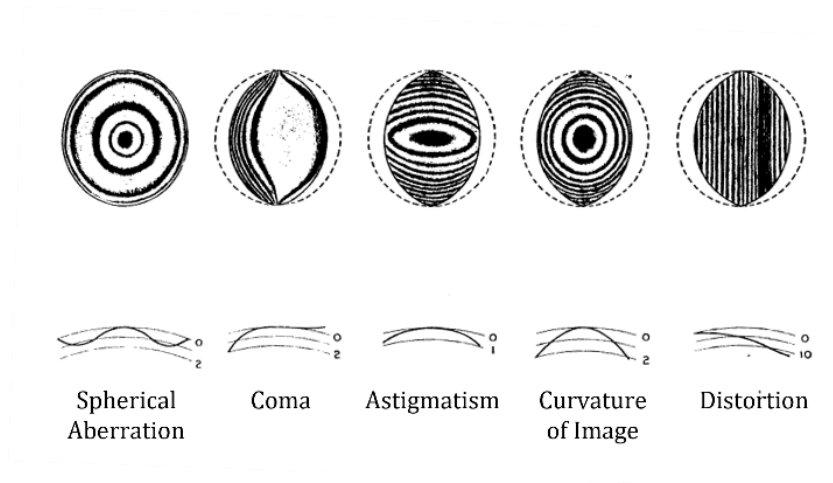


Figure 6. Example of an output of Twyman's Experiment. The images are different ways in which a lens that is being tested by the interferometer can be incorrect or broken. The top image is what the interferometer shows the user. The bottom part of the image is how to interpret the output of the machine. Figure taken from Ref. [8].

1.3.2.3. Modified Twyman-Green Interferometers

There have been multiple experiments [9, 10, 11] that have used a modified Twyman-Green interferometer to aid in the research. One of these experiments [12] was performed by Lawrence Steimle and Yaujen Wang to test filters for the Hubble Telescope. The researchers realized that the original Twyman-Green interferometer that was being used for the experiment was only able to give a bandwidth of 400 to 700 nm. The tests that needed to be done needed a bandwidth as low as 200 nm and as high as 1100 nm. Another problem with the original design is the cost. Other designs at the time required other types of mirrors (off axis parabolic mirrors) that were expensive. This would be to forgo the use of a collimating lens in the experimental setup. The researchers were trying to find a way of limiting the cost of the system.

To fix the problem with the expensive mirrors, the group changed the layout of the interferometer, and used a spherical mirror instead. An image of their design can be seen in Figure 7. This mirror allows the beam to travel in a way that the off axis parabolic mirrors are not necessary. This was done by using a spherical mirror to both collimate the beam and un-collimate the beam. To solve the problem with the precision of the interferometer, the group used a CCD Camera, or Charged Coupled Device Camera. This camera allowed the researchers to have the desired performance of the interferometer.

Using these modifications, it was possible to get a more detailed measurements of the filter that was being tested. This is due to the range of the bandwidth being increased from 400-700 nm to 200-1100 nm. This increase came from using the silicon-based CCD as the data capturing instrument. The new design was also more convenient to use, as the room did not need to be as dark as there was a cover for the apparatus. This was possible due to the monitor that was showing the data was separate from the system itself. This property also made the system easier to use. The 200-1100 nm range of bandwidth was able to be achieved. Other advances in the Twyman Green Interferometer involved using a laser beam as the light source instead of white light.

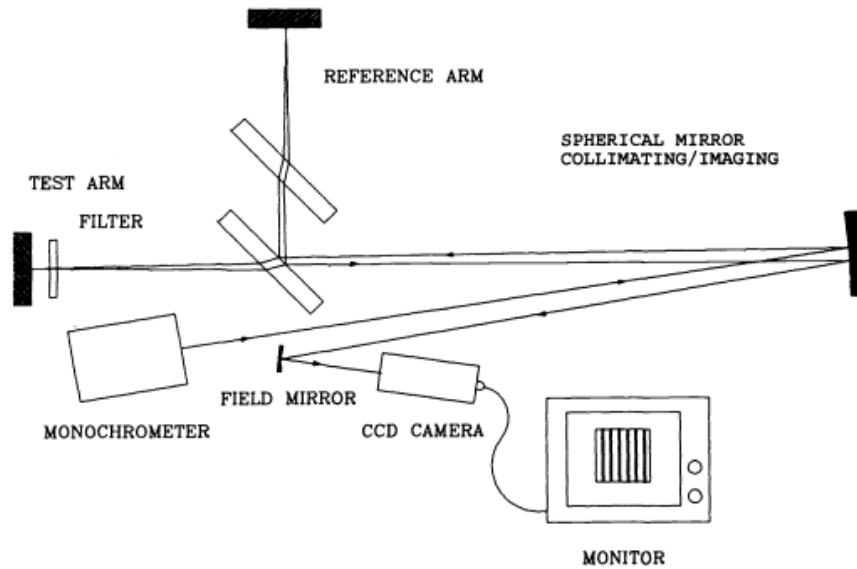


Figure 7. Diagram of the design of the experiment by Steimle and Wang. The light source starts at the monochromator and reflects off the spherical mirror. The light then travels a similar line to the original Twyman Green interferometer. The recombined beam then reflects off the spherical mirror again, and travels to the CCD Camera, where the data is interpreted. Figure taken from Ref. [12].

1.3.2.4. Interferometers Using Lasers

After their invention [13] in 1960, lasers started becoming a popular light source in experiments [14, 15] that use interferometry. This is because of the coherence length of a laser verses that of white light. Coherence length is the distance in which two beams of light from the same source would be highly correlated. That means that if the difference in distance traveled between the two beams is greater than the coherence length of the light, the two beams would not give any information when recombined. Due to this, the difference between the path lengths of the beams must be less than the coherence length of the light source. The coherence length of white light is on the order of a micrometer, verses on the order of a meter for a laser. This means that the path lengths do not have to be as precisely matched with a laser as they do when white light is the light source being used.

One instance of a laser interferometer comes from an experiment [6] performed by C. Tien, Y. Lyu, and S. Jyu in 2008. This experiment involved measuring the surface flatness of thin

films using an interferometer with a laser as the light source for the experiment. The experiment setup can be seen in Figure 8.

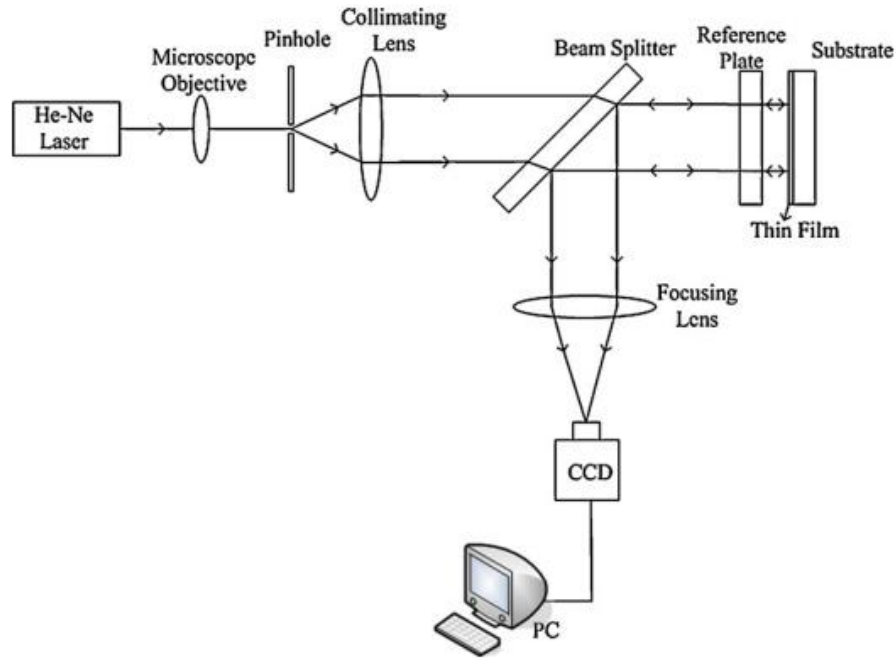


Figure 8. Experimental setup from Tien, Lyu, and Jyu's experiment. The laser beam started from the source on the left, then traveled to the collimating lens, where the cross sectional area of the beam increased. The beam then traveled through a beam splitter where it traveled to a reference plate and the testing surface. The beam then came back to the beam splitter, and reflected to the CCD camera, that was used to collect the data and send it to the computer, where the data was analyzed. Figure taken from Ref. [6].

Tests were done on TiO_2 films that were deposited on 25.4 mm B270 glass substrates. The deposition rate of the vacuum deposition system that was used was 0.48 nm/s, and the pressure inside of the system was 5.4×10^{-4} Torr. The thickness of the films was roughly 200 – 400 nm. A topography of the film can be seen in Figure 9. The experiment was successfully able to determine the flatness of the films that were used, with an uncertainty of 3.89% at a confidence interval of 95%.

Another modification that was made to the Twyman-Green interferometer was the implementation of a moving reference mirror. This new interferometer design is known as a phase shifting interferometer.

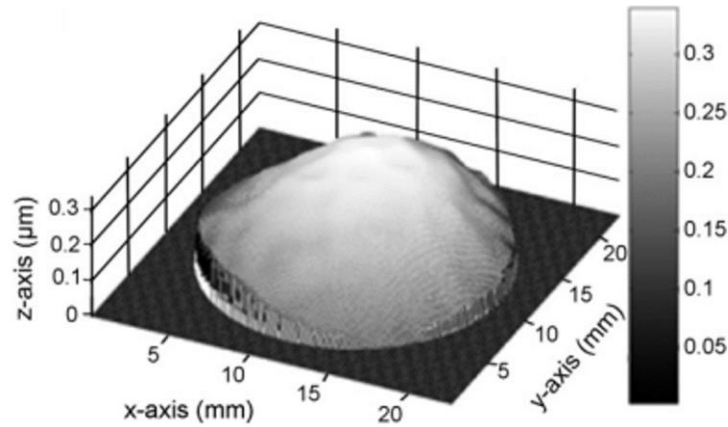


Figure 9. 3-D Topography of one of the films from the Tien Experiment. This film was one of the films used to test the interferometer in the experiment. The reference plate that was used had a flatness of $\lambda/20$. Figure taken from Ref. [6].

1.3.2.5. Phase Shifting Interferometer

A phase shifting interferometer works by moving the reference mirror in a controlled manner. This is usually done using a computer-controlled circuit to apply a voltage to piezoelectric stacks, which can move the mirror with sub-nanometer precision. Piezo electrics expand in one direction when a voltage is applied to them, and as the voltage is increased, the distance expanded is also increased. Phase Shifting Interferometry is used in multiple experiments [16, 17, 18], including measuring the topography of a surface and measuring a specimen in biology applications.

In 1979, Ronald Grosso and Robert Crane developed a phase shifting interferometer used in an experiment [5] to study the topography of a test surface. The experiment used a modified Twyman-Green interferometer that can be seen in Figure 10. The interferometer works by splitting a wide beam, having one of the beams travels to the test surface and one to the reference mirror. The beams recombine and then travel to the interference plane, where the interference pattern of the two beams is studied.

To get the surface topography of the test surface, either the surface or the reference mirror needs to move. When the reference mirror moves, the interference pattern changes. If the experimenter were to look at one individual point, and plot to intensity of the light at that

point, a sine function would be produced. The phase shift of the sine function from every point gives the experimenter the topography.

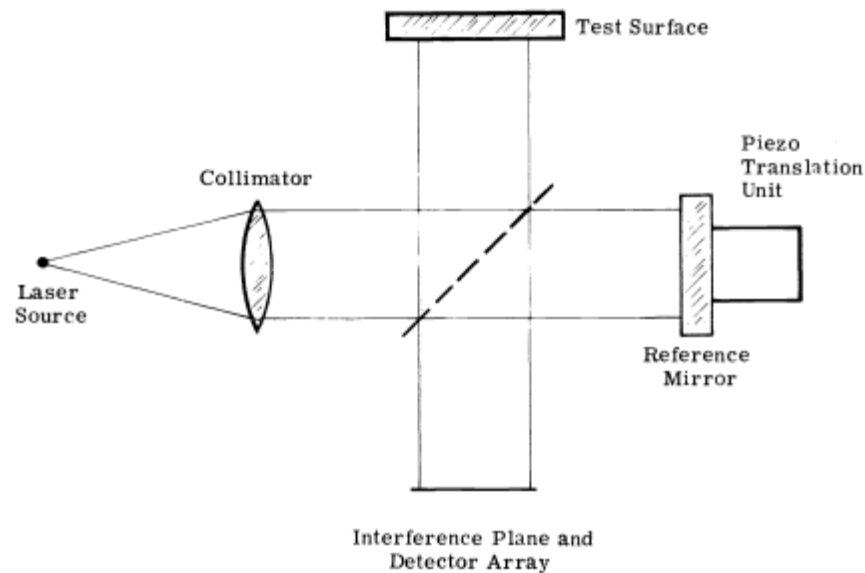


Figure 10. Diagram of a general phase shift interferometer. The laser increases to the desired cross sectional area and passes through the beam splitter. The beam then splits, and one travels to the surface that is being tested, and the other to the reference mirror. The beams then come back to the beam splitter, recombine, and travel as one beam to the Interference Plane. Figure taken from Ref. [5].

Using this setup, Grosso and Crane produced a surface topography of multiple test surfaces with an uncertainty of less than 0.01 wavelengths. The experiment was able to achieve an uncertainty of less than 0.01λ . The wavelength of the light source in this experiment was 633 nm. Some of the results of the experiment can be seen in Figure 11. The apparatus was used to get a topography of the surface with the uncertainty mentioned above.

There are many different surfaces that might need to be created with a high level of precision in mind. Thin films are an example of these surfaces. Using phase shifting interferometry, as well as laser interferometry, makes it possible to test the surface to make sure it has the desired measurements. One of these surfaces is thin metal films.

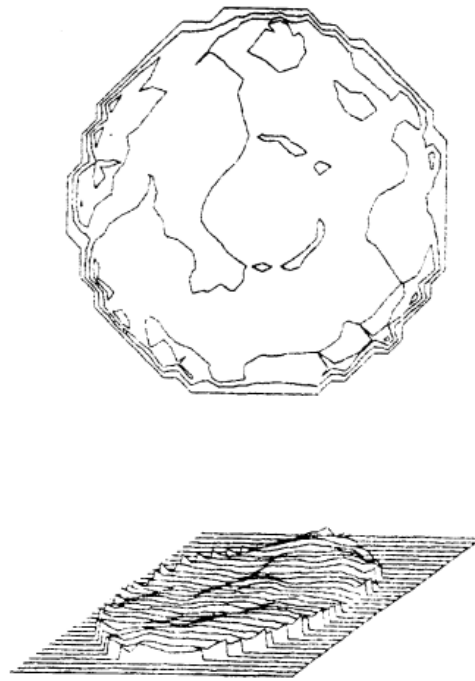


Figure 11. Images from Grosso and Crane's phase shifting interferometer. The figure shows a topography of one of the test mirrors that was used to test the apparatus. Figure taken from Ref. [5].

1.4. *Thin Metal Films*

1.4.1. Introduction to Thin metal films

Thin metal films are metal sheets with a height usually on the order of nanometers. The main use of these thin metal films is in electronics. Some of the use cases in electronics are printed circuit boards and semiconductors. These films are created using vacuum deposition [19], which can produce different types of metal films. When creating films, there are aspects of the creation that can be changed, including the deposition rate, which is the amount of metal deposited per second, and the pressure of the chamber the metal is created in. Changing these aspects, as well as others, can alter the film itself. To see what these changes do to the metal film, the topography of the film can be evaluated using a phase shifting interferometer.

1.4.2. Experiments on Thin Metal Films

Using an interferometer to measure properties of Thin Metal Films has been done in many different experiments [20, 21]. One of these experiments [22] was done by Young-Sik Ghim

and Seung-Woo Kim in 2009. Their experiment involved using white light phase shifting interferometry to study thin metal films to help the microelectronics industry. Their apparatus, which is similar to that in Figure 10, was used to study two silicon dioxide thin film samples on silicon substrates. The substrates were 350 by 400 μm and 150 by 150 μm . The films were about 4 and 3 μm respectively. The experiment was successfully able to successfully give a 3D rendering of the thin films and substrates that were used in the experiment. The 3D rendering comes from getting a topography of both the substrate that was used in the experiment, as well as the film that was produced. An image of the results can be seen in Figure 12. The experiment was successful at achieving a topography of a thin metal film.

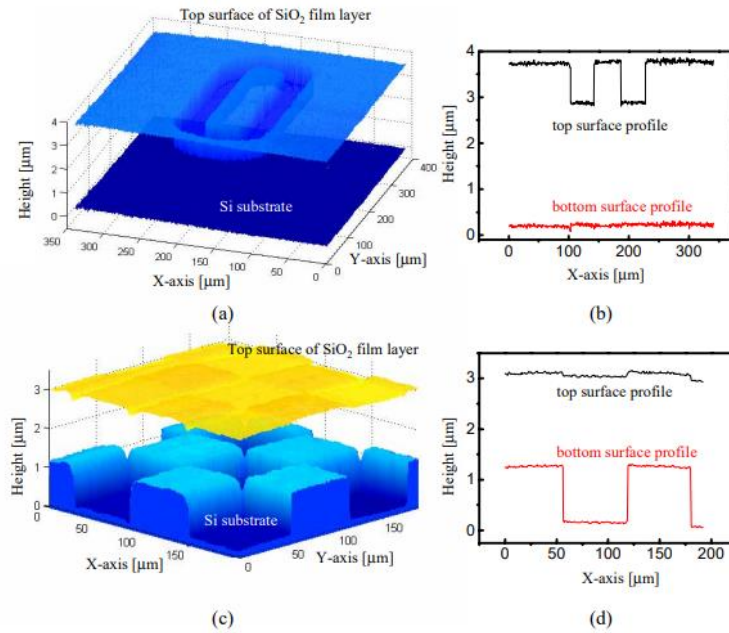


Figure 12. Surface topography of SiO₂ films. (a) and (c) are 3D renderings of the films and substrates. The graphs (b) and (d) are side profiles of the top and bottom of the thin metal film. The surfaces were measured using phase shifting interferometry. The precision of the interferometer was 500 nm Figure taken from Ref. [22].

1.5. Houghton University Thin Metal Films Laboratory

1.5.1. Houghton University Laser Interferometer

The interferometer at Houghton University is a modified Twyman-Green interferometer, with some modifications. One of the biggest modifications involves the increasing size of the

beam of light. Instead of having the laser increase in size, then passes through the beam splitter, the laser beam passes through a diverging lens, and then passes straight into the beam splitter. The beam then increases in size as it travels down the two arms of the apparatus. The beams are then collimated right before the mirror and test sample. The beam then reflects off the surfaces, passes through the collimating lenses to start decreasing the size of the beam until it enters the beam splitter. The recombined beam then grows until it reaches the semitransparent screen, where a webcam takes a picture of the interference pattern once every second. The apparatus also uses 3 piezoelectric ceramic stacks to move the reference mirror.

1.5.2. Other Thin Metal Film experiments at Houghton University

Part of the Physics Department at Houghton University is currently working on a laboratory to create and test the properties of thin metal films. The goal of this laboratory is to be able to take different tools that are at other locations and have students build them in a cost-effective way. This would then allow students to test different ideas with thin metal films. Currently, there are students working on four different projects.

A vacuum deposition chamber [23] is being built to create thin metal films with different deposition parameters. After these films are created, the phase shifting laser interferometer will be used to determine the thickness and topography of the films. To determine the crystal structure of the film, a, X-Ray Diffractometer [24] chamber and a scanning tunneling microscope are being constructed.

The goal of this lab is to create thin metal films with different properties using the deposition chamber and see how different deposition parameters will affect the structure of the film. These parameters include the pressure inside the chamber, the temperature of the sample, and the deposition rate of the material. Then, the other experiments in the laboratory will be used to evaluate the structure of the film. The other equipment in the laboratory will also be able to see how the crystal structure of the film is affected by changes to the film that could happen in different uses of these thin metal films.

This information could then be used by other researchers to see the electronic properties of films with certain crystal structures. This would then allow manufacturers to be able to know how to make their films to have these different properties, allowing them to create more efficient products.

Chapter 2

THEORY

2.1. *Introduction*

In a phase shifting interferometer, the main theoretical idea being implemented in the experiment is the use of light and the interference between two beams of light. Being able to understand how the beams of light interfere with each other relative to the surface being tested, and the position of the reference mirror is crucial to producing a topographical image of the test surface.

2.2. *Light and Interference*

2.2.1. Single Beam of Light

Light is an electromagnetic wave. In SI units, the Poynting vector for an electromagnetic wave is defined as:

$$\vec{S} \equiv \frac{1}{\mu_0} \vec{E} \times \vec{B} \quad (1)$$

where \vec{S} is the power of the electromagnetic wave per unit of area perpendicular to \vec{S} , μ_0 is the permeability of free space, \vec{E} is the electric field, and \vec{B} is the magnetic field. In a homogenous, linear, anisotropic medium the electric and magnetic fields are always perpendicular, making it possible to write the magnitude of the Poynting vector as:

$$S = \frac{EB}{\mu_0} \quad (2)$$

where S , E , and B are the magnitudes of their respective vectors. It is also known that:

$$B = E/c \quad (3)$$

where c is the speed of light in a vacuum. Using Equation (3), Equation (2) can be rewritten as:

$$S = \frac{E^2}{\mu_0 c}. \quad (4)$$

From this, it is possible to see that S is related to E^2 as both μ_0 and c are constants.

The average of S will be used to get the intensity from Equation (4). The solution to the wave equation is needed to get the average of S . The wave equation is:

$$\frac{\partial^2 E}{\partial t^2} = c^2 \frac{\partial^2 E}{\partial x^2} \quad (5)$$

where x is the distance from the origin along the path of the wave and t is time in seconds. The solution to this equation is a sinusoidal function of:

$$E = E_{\max} \sin\left(\frac{2\pi}{\lambda}(x - ct) + \phi\right) \quad (6)$$

where E_{\max} is the maximum of the wave, ϕ of the phase shift of the wave, and λ is the wavelength of the wave. When the $\frac{2\pi}{\lambda}$ is distributed through the equation, it is possible to define $\omega = \frac{2\pi c}{\lambda}$. The value S is the power at an instant in time, but the overall intensity of the wave is the average of Equation (6). The average of Equation (6) squared is E_{\max} multiplied by $\frac{1}{2}$. Using this, it is now possible to get the intensity from Equation (4), which is:

$$I = S_{\text{avg}} = \frac{E_{\max}^2}{2\mu_0 c} \quad (7)$$

where I is the intensity of the electromagnetic wave, or in our case, the light. This is for one source of light, but there are two laser beams that interfere with each other.

2.2.2. Multiple Beams of Light

Now consider two beams of light, as shown in Figure 13. The origin is defined such that the light traveling to sample mirror C has a phase shift of 0. Therefore, the phase shift of the beam traveling to reference mirror D is proportional to the difference in the travel distance of the two beams, $2(-y + y_s)$, where y_s is the height of the portion of the sample the light reflects off. This means that the interference that is shown on the semitransparent screen is not one, but two beams of light that have been recombined by the beam splitter. For every position on the sample, y_s will be different based on the height of the sample at the position. The light intensity of a given position on the screen will depend on the corresponding position on the sample.

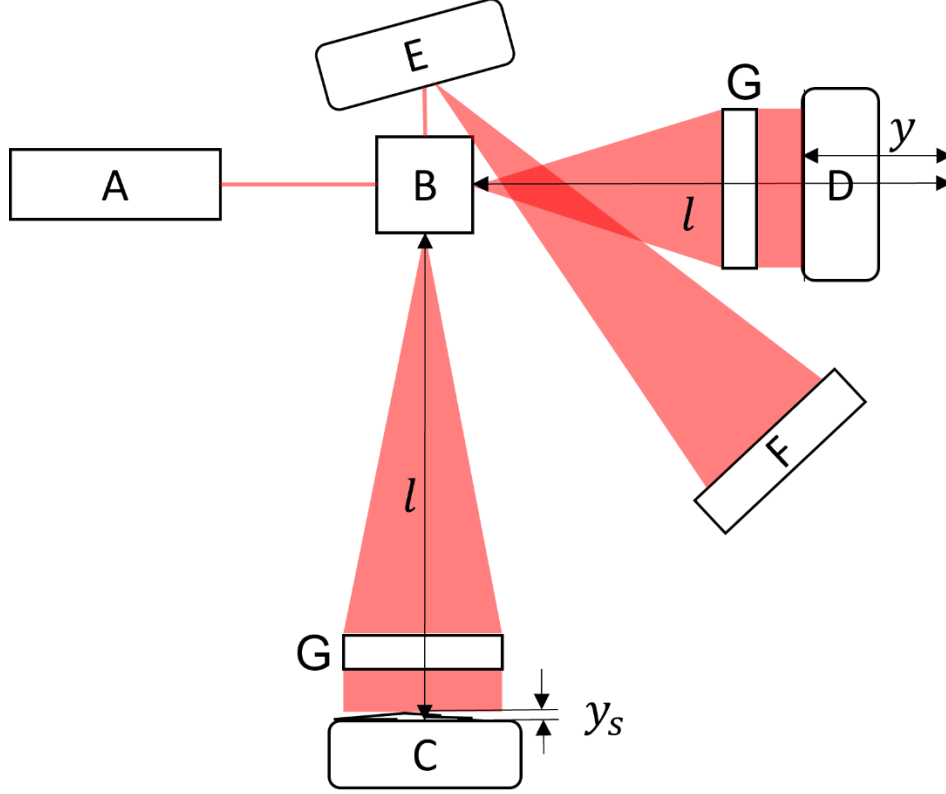


Figure 13. A simplified image of the interferometer at Houghton. A is the laser, B is a beam splitter, C is the sample, D is the reference mirror, E is a mirror and lens setup that directs the beam to F, which is the screen that is used to see the outcome of the experiment. The rectangles labeled G are the collimating lenses used to collimate the beams of light. The laser beam goes through the beam splitter, gets sent to both the sample and reference mirror, then back to the beam splitter to recombine then to the other mirror and finally, the screen. The distance between the two lines on the arm D is on, is the difference in length between the two arms. y_s is the height of the sample at any point.

The phase shift, ϕ , now needs to be written in terms of the known distances, which is:

$$\phi = 2(-y + y_s) \frac{2\pi}{\lambda} + 2\pi n \quad (8)$$

where n is any integer. The last term is necessary because Equation (6) is periodic and therefore has an infinite number of solutions. The last term can be accounted for by defining $y_{s,n} \equiv y_s + \frac{n\lambda}{2}$. Therefore, the phase shift is $\phi = 2(-y + y_{s,n}) \frac{2\pi}{\lambda}$. When two waves interfere with each other, the two electric fields are added together. That means that when the two beams of light come together, we get the equation:

$$E_{\text{total}} = E_{\text{max}} \sin\left(\frac{2\pi}{\lambda}x - \omega t\right) + E_{\text{max}} \sin\left(\frac{2\pi}{\lambda}x - \omega t + \frac{2\pi}{\lambda}2(-y + y_{s,n})\right) \quad (9)$$

where E_{total} is the combination of the two equations. This simplifies to:

$$E_{\text{total}} = 2E_{\text{max}} \cos\left(\frac{2\pi}{\lambda}(-y + y_{s,n})\right) \sin\left(\frac{2\pi}{\lambda}x - \omega t + \frac{2\pi}{\lambda}(-y + y_{s,n})\right). \quad (10)$$

This equation is used in Equation (4) to work out the intensity of the two beams of light combined. First, the function needs to be squared, then the time average of the function needs to be determined. The cosine part of the function is a constant. The sine part of the function, due to it being squared, has an average of $\frac{1}{2}$. This means that:

$$I_{\text{total}} = \frac{E_{\text{max}}^2}{\mu_0 c} 2 \cos^2\left(\frac{2\pi}{\lambda}(-y + y_{s,n})\right). \quad (11)$$

This is the total intensity of a single point of light. This translates to a single point on the surface that is being tested. On top of this, due to some light from outside the experiment leaking into the system, there is some constant intensity, D , in addition to the intensity from the two interfering beams:

$$I_{\text{total}} = \frac{E_{\text{max}}^2}{\mu_0 c} 2 \cos^2\left(\frac{2\pi}{\lambda}(-y + y_{s,n})\right) + D \quad (12)$$

where D is a stand-in for noise from outside the experiment. This can be simplified to a cosine function:

$$I_{\text{total}} = \frac{A}{2} \cos\left(\frac{4\pi}{\lambda}(y + y_{s,n})\right) + D' \quad (13)$$

where $A \equiv 2 \frac{E_{\text{max}}^2}{\mu_0 c}$ and $D' \equiv D + \frac{E_{\text{max}}^2}{\mu_0 c}$. The value $y_{s,n}$ can be determined by moving the mirror at a constant speed, v , such that $y = vt$, then plotting the total intensity vs. time, then fitting the data to a cosine function:

$$I_{\text{total}} = A \cos(bt + c) + D' \quad (14)$$

where $b \equiv \frac{4\pi}{\lambda}v$ and $c \equiv \frac{4\pi}{\lambda}y_{s,n}$. The height of the surface sample y_s , depends on $y_{s,n}$ according to equation (14).

To produce a surface topography of the sample, it is not necessary to determine the absolute value of y_s at any position on the sample. It is only necessary to determine relative values of y_s , which can be accomplished by assuming that the sample surface is smoothly varying. In that case, relative values of y_s can be determined by choosing each n so as to minimize the difference between the values of y_s at adjacent positions along the sample.

Chapter 3

APPARATUS

3.1. *Layout of the Apparatus*

A picture of the apparatus, as well as the path of laser beam can be seen in Figure 14. The laser that is being used is a Coherent VHK 3.0 mW, 635 nm Circular Beam Visible Laser Diode (model no. 0221-699-01). The beam of light starts at the laser, then travels 21 cm and passes through a 6 mm diameter diverging lens with a focal length of 6mm to increase the cross-sectional area of the beam. The beam then passes through the beam splitter. The beam splitter is a 1 inch cube beam splitter that allows half of the light to pass through, and the other half will reflect off the surface. The half-silvered surface of the beam splitter makes a 45° angle with the beam of light, allowing the part of the beam that is reflected to be at a 90° angle from the other part of the beam.

From the beam splitter, the two beams then travel 482 mm in their respective directions, until they reach a diameter of 83 mm. The beams then both travel through a collimating lens with a 90 mm diameter and a focal length of 500 mm. After going through the collimating lens, one of the beams travels to the sample, and the other travels to the reference mirror.

The other beam passes from the other collimating lens to the reference mirror. The reference mirror is a 102 mm $\lambda/10$ flat mirror. The mirror is inside an aluminum cylinder to keep objects from coming in contact with the surface. The mirror and mirror holder are moved using 3 Noliac NAC2024 piezoelectric ceramic stacks that are roughly 2 mm thick. These stacks move the mirror up to 883 nm away parallel to the beam path with sub-nanometer precision. The mirror holder is pressed into these stacks by 4 rubber blocks from a Pllieay B-002B rubber ball. The stacks are in between the mirror holder and an Edmund Optics 4.5 inch angle mirror mount. An image of the mirror holder, and how it is held up while allowing movement can be seen in Figure 15.

The piezoelectric ceramic stacks expand when a voltage passes through them. The circuit diagram that shows how the piezoelectric stacks are powered is shown in Figure 16. The

voltage comes from a National Instruments DAQ. The voltage from the DAQ is shifted down by a -2.5 V power supply. This has the input of the BB OPA453T operation amplifier range from -2.5 – 2.5 V. The voltage output of the noninverting op amp can be calculated using the equation:

$$V_{\text{out}} = \left(1 + \frac{R_1}{R_2}\right) V_{\text{in}} \quad (15)$$

where R_1 is 94 M Ω and R_2 is 7.7 M Ω . The -30 V and 30 V power supplies cap the minimum and maximum output at -30 V to 30 V. The positive terminal of the stacks is connected to the output of the operational amplifier circuit, and the negative terminal is connected to a -30 V terminal. This means that the voltage across the stacks is proportional to the 0 - 5 V input voltage and goes from 0 – 60 V.

The viewing screen is a semitransparent screen made from white copy paper that the recombined beam illuminates. The interference pattern of the two beams, which is seen on the screen, is used to determine the topography of the sample. A 2 MP Microsoft Q2F-00013 MAIN-31891 LifeCam Studio webcam is used to take picture of the interference pattern once every second. This is done using the software Yawcam.

3.2. Mechanical Vibration Isolation

When the system is operational, vibrations coming from outside the system can ruin the data that is collected. To solve this, there are multiple ways of limiting vibrations built into the system. One of these is the housing. The housing is a 959 mm x 958 mm x 2134 mm box that surrounds the entire system. This box is designed to be easily disassembled by using magnets to hold the pieces of plastic to the metal frame. The housing is used to limit the wind from the building's air circulation unit from interfering with the system. A picture of the housing surrounding the system can be seen in Figure 17.

Another system that is being used to limit the number of vibrations that effect the interferometer are the springs that the table is hanging from. These springs are mounted to the housing and can also be seen in Figure 17. The springs limit the resonant frequency of the system to about 1 Hz. This value is lower than the building's resonant frequency. The

lower vibration of the system is then lowered further using the eddy current damping system.

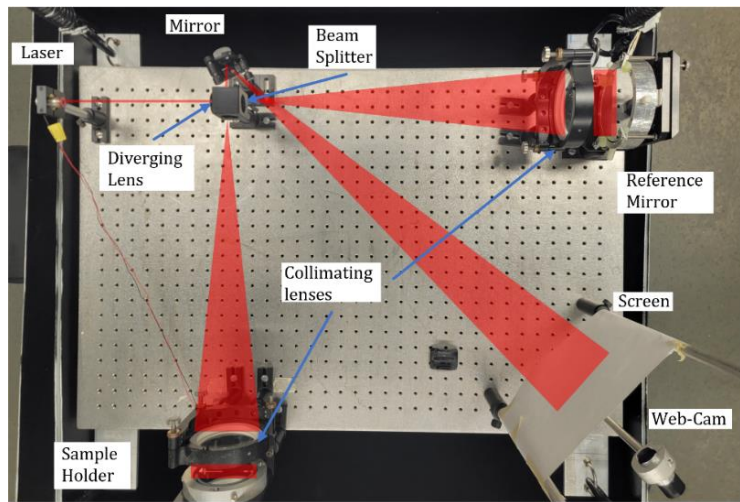


Figure 14. Picture of the Houghton University interferometer. The path of the beam has been drawn over the picture in red. The laser is in the top right of the image and the beam splitter and one of the mirrors is in the top middle of the picture. The reference mirror is in the top left, and the sample holder is in the bottom left of the image. The screen that shows the interference pattern is in the bottom right of the image. The distance between each hole on the table is 1 in. The table being used is 91.4 cm long by 61 cm wide.

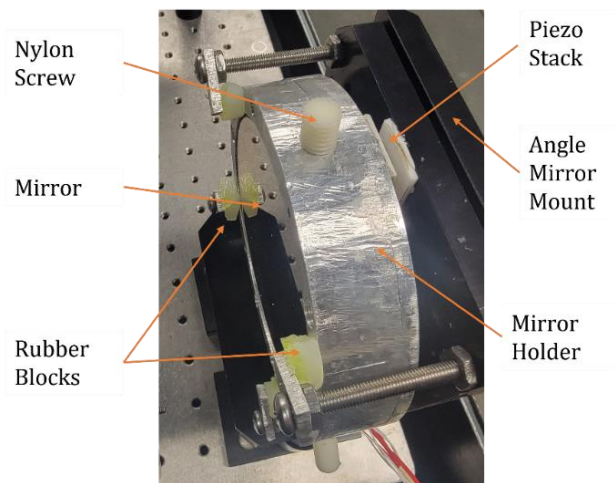


Figure 15. An image of the holder of the reference mirror. The mirror is held in place by four 2 inch screws that with pieces of metal on them that act as "arms". These arms are used to hold the mirror in place, so it does not fall. In between the arms are the mirror holder, there are pieces of rubber. These pieces of rubber allow the movement of the mirror but keep it in place when stationary.

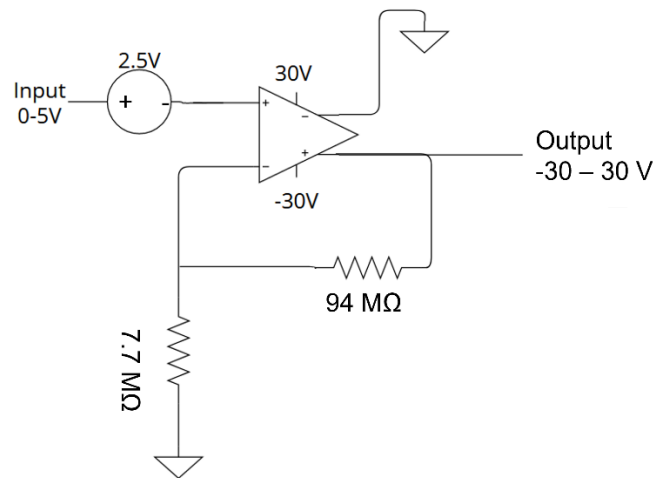


Figure 16. A circuit diagram of the electronics used to move the mirror. The input is from the computer program that outputs from 0-5 V. The speed of the change from 0-5 V is determined by the user. The output goes to the 3 piezoelectric ceramic stacks, to move the reference mirror with sub nanometer precision. The negative terminals on the stacks are at -30 V, making the output act like 0 – 60 V.

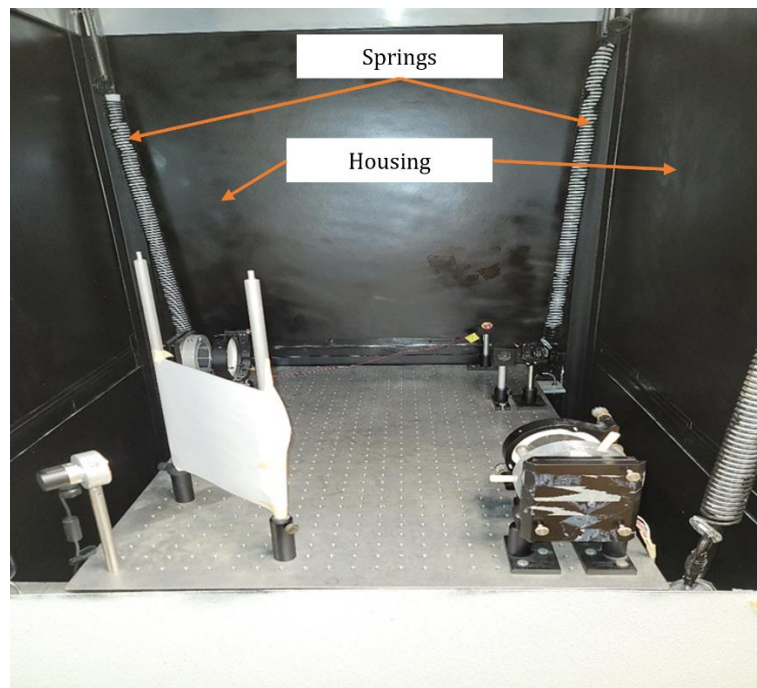


Figure 17. An image showing the housing and the springs. The housing is used to limit the amount of wind that can affect the system. The springs allow the table, and everything attached to it moves together.

The eddy current damping system is another way of decreasing the vibrations of the system. The damping system consists of a 635 mm by 660 mm box that surrounds a section of the table. There are 28 7.6 x 1.2 x 0.6 cm neodymium magnets attached to the inside of the box. The eddy current damping system can be seen in Figure 18 Figure 19. When the box passes through the magnetic field, a current is induced in the table. This current causes a force the in the opposite direction of the movement. This force causes the movement of the table to slow down. The slowing down of the table leads to less vibrations affecting the system. Both the box used for eddy current damping, as well as the frame, sit on four 4 x 4 x 7/8 in. EVA anti-vibration pads. These pads absorb some of the movement of the system, limiting the movement. All these different systems together help to reduce the effect of outside vibration on the system.

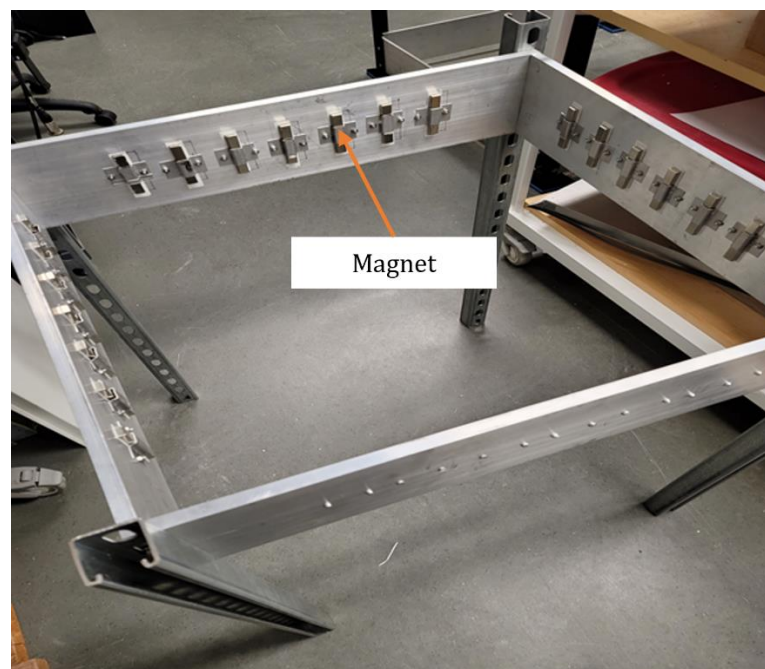


Figure 18. The Eddy Current Damping box. The system shown is used to limit the amount of movement of the interferometer. The 28 neodymium magnets are used to create a magnetic field when an object moves into the box. The magnetic field induces a current in the object and creates a force in the opposite direction of the movement.

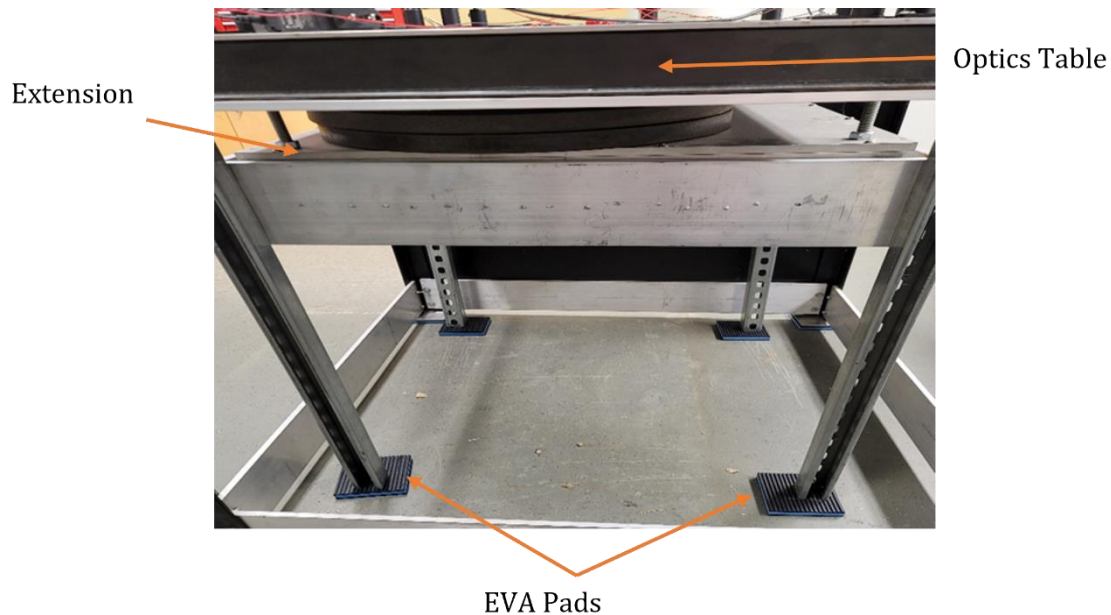


Figure 19. The section of the table that is inside the Eddy Current Damping Box. The table has an extension that goes down into the box. As this section of the table goes into the box, the speed of the movement is slowed to limit the vibrations in the system.

3.3. Collecting and Analyzing the Data

To collect the data from the interferometer, a NI USB-6008 is controlled by a LabVIEW program that has the device output a voltage from 0-5 V, increasing constantly over 100 s. This voltage is then inputted into the circuit shown in Figure 16, which using the operational amplifier, outputs a voltage from 0-60 V. This voltage is proportional to the voltage that is the input of the circuit, to the piezoelectric ceramic stacks. These stacks then move the reference mirror at a constant velocity. As the reference mirror is moving, the webcam, operated by the program Yawcam, takes a picture of the interference pattern once a second for 100 s. These pictures are then analyzed to get the surface topography of the sample. A flow chart of the data processing can be seen in Figure 20.

After the data is collected, the data analysis is done in different LabVIEW codes to make sure each step is working. The first step is to find the intensity of each pixel in every picture. This is done by changing the pictures from color images to gray scale. To make this change, first, the gamma compression done by the camera needs to be undone. This can be done by using the equation:

$$C_{\text{linear}} = \begin{cases} \frac{C_{\text{srgb}}}{12.92} & \text{if } C_{\text{srgb}} \leq 0.04045 \\ \left(\frac{C_{\text{srgb}} + 0.055}{1.055} \right)^{2.4} & \text{otherwise} \end{cases} \quad (16)$$

where C_{linear} is the value of each color, red, green, and blue, after the gamma compression is undone, and C_{srgb} is the value of the colors before the compression is undone. The next step in converting to grayscale is taking these new values for each pixel and multiplying them by constants. These constants can be seen in the equation:

$$0.2126 R_{\text{linear}} + 0.7152 G_{\text{linear}} + 0.0722 B_{\text{linear}} = gr_{\text{linear}} \quad (17)$$

where R_{linear} is the value of red in the pixel, G_{linear} is the value of green, B_{linear} is the value of blue, and gr_{linear} is the intensity of the gray pixel produced by converting the image to gray scale. Currently, only the second step is being done. After completing this step, the data is a group of 100 arrays that are 640x480 in size and have the intensity of each pixel for each picture.

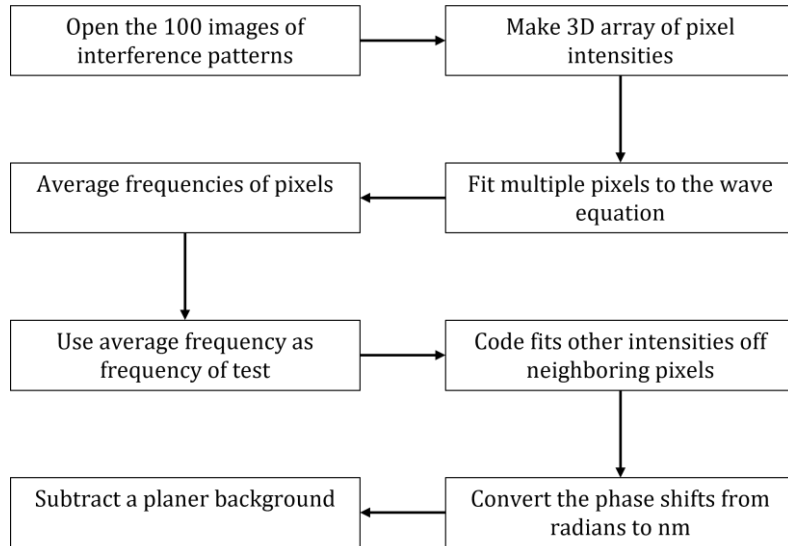


Figure 20. A flow chart of how the data being processed. After the data are collected, the data are then taken through the steps above to determine the topography of the thin metal film. The topography produced is in nm.

After the intensity values are found, the next step is to fit the sine function (12) to each of the pixels throughout every picture. First, the sine function of the center pixel is fitted using a

separate program to determine the value of the frequency of the sine function. After going through multiple tests, it was determined that for the code to fit each of the values, the frequency needs to be known. If the frequency was not a constant for the code, LabVIEW would not create the correct sine function. This in turn would not produce the correct phase shift. This is due to the fact that a set of noisy data points can sometimes be fit to multiple equations with a different frequency. Because the entire mirror moves at the same constant speed, the frequency of one pixel is equal to the frequency of the other pixels.

After the parameters for one pixel are found, it is time to fit a sine wave to all the other pixels. This is done by fitting the pixels from the center of the picture to the outside. This is done so the program starts where the interference pattern would exist, instead of the outside of the image, where there is no interference pattern. The important value from each of these sine waves is the parameter c from Equation (14), which if plotted in an intensity plot, is the topography of the sample surface. To find this parameter faster, the adjacent pixel's sine wave parameters are used as the initial guess for the sine wave fit of the next pixel.

When all the c parameters are found for each pixel, the values are in radians. To convert them from radians to nanometers, the equation:

$$y_s = \phi \frac{635 \text{ nm}}{2(2\pi)} \quad (18)$$

is used, which is from equation (14). The equation includes the $2(2\pi)$ part because if the path length change goes from a peak to a peak, the c parameter changes by (2π) , and because of the beam reflecting, the change in the pathlength would be divided by 2. This equation is a reverse of Equation (8), as this converts ϕ from radians to nanometers. This equation outputs the value of the c parameters in nanometers. The next step of the data manipulation is to subtract the background from the data.

The background subtraction is done to counteract any small angle the mirror might be at. This is done by first finding the average for each column in the data frame. A linear regression is then done on the averages of all the columns. This linear regression is $f(x)$ in Figure 21. This function is then subtracted from each value of each column in the data frame. This method is then repeated with all the rows in the data frame.

The final step of the data manipulation is done by finding the minimum value of the array. This value is then subtracted from every pixel in the array. This is done to have the same reference point for every test. The output of this final step is the topography of the sample that is being tested.

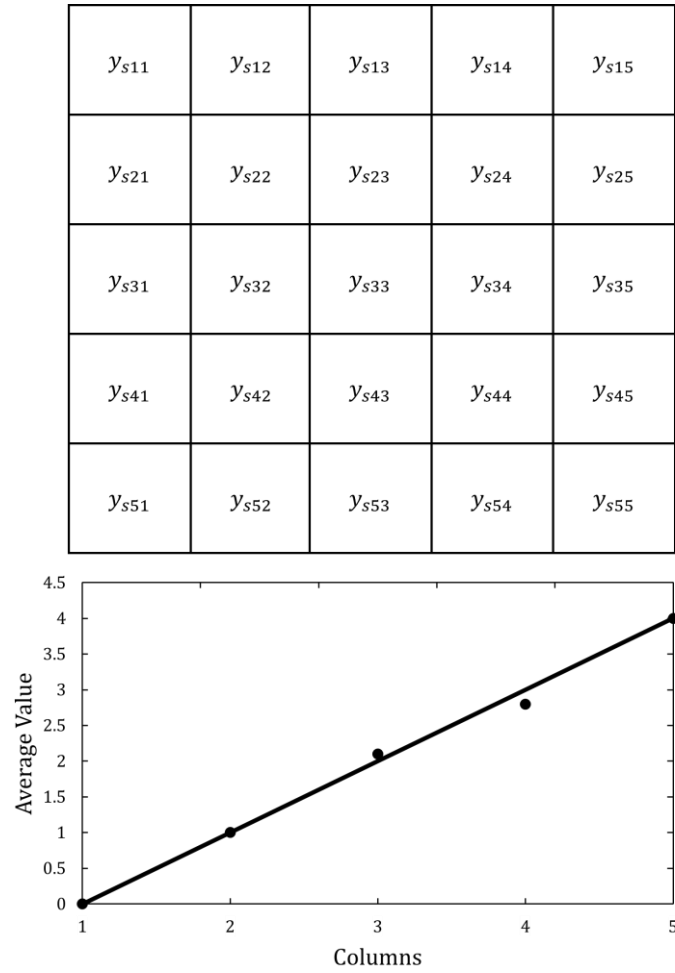


Figure 21. Diagram showing the background subtraction done to the topography. The 5x5 array represents the array of values that is the topography of the surface. The average of each column is found and plotted. A linear regression is done to find $f(x)$, which is the line in the function. This function is subtracted from every value of each column in the data frame.

Chapter 4

RESULTS

4.1. Topography of Mirror

Preliminary tests were conducted with a 75 mm $\lambda/10$ flat mirror in place of the sample. The interferometer was able to get a partial topography of this mirror. An interference pattern of the image, as well as the area of the interference pattern that was tested, is shown in Figure 22.

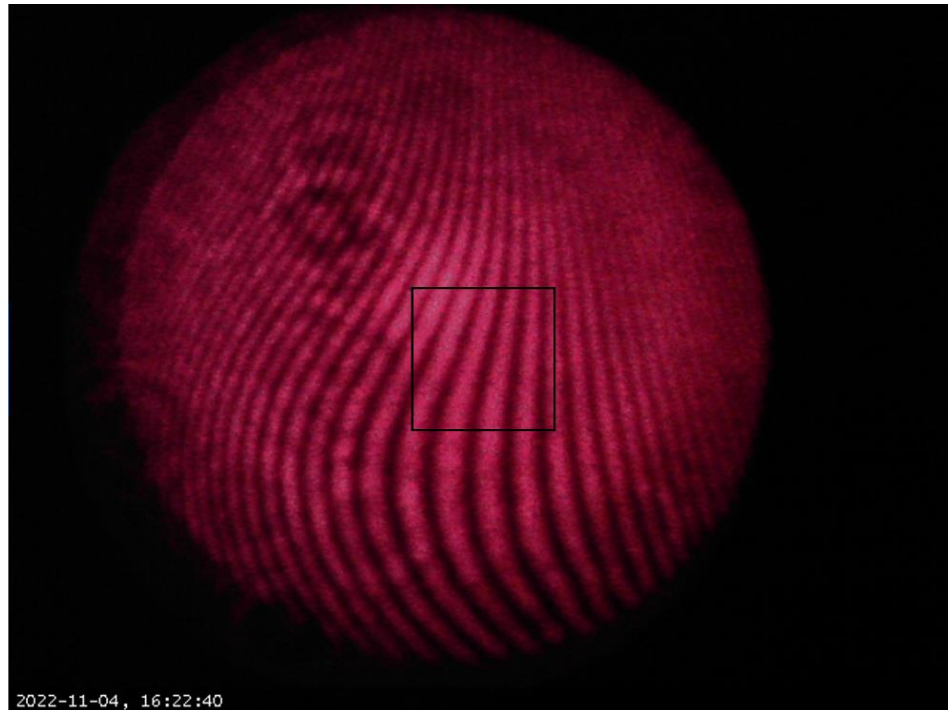


Figure 22. Picture of an interference pattern and the area being tested. The area that is being tested is inside the black square.

The smaller circles that can be seen around the interference pattern are unaffected by the position of the reference mirror and therefore do not affect anything but the offset and amplitude of the sine function that is being fit. This means that any of these blips, or any other noise that might be visible in the test, do not affect the data or the topography from the test. To get the topography, 100 pictures like the one shown in Figure 22. Plots of the

intensity of the center pixel from last year and this year are shown in Figure 23 and Figure 24, respectively. The fit of the sine function is not as good as this year's test. The difference in the sine function fitting came from altering the mount of the reference mirror.

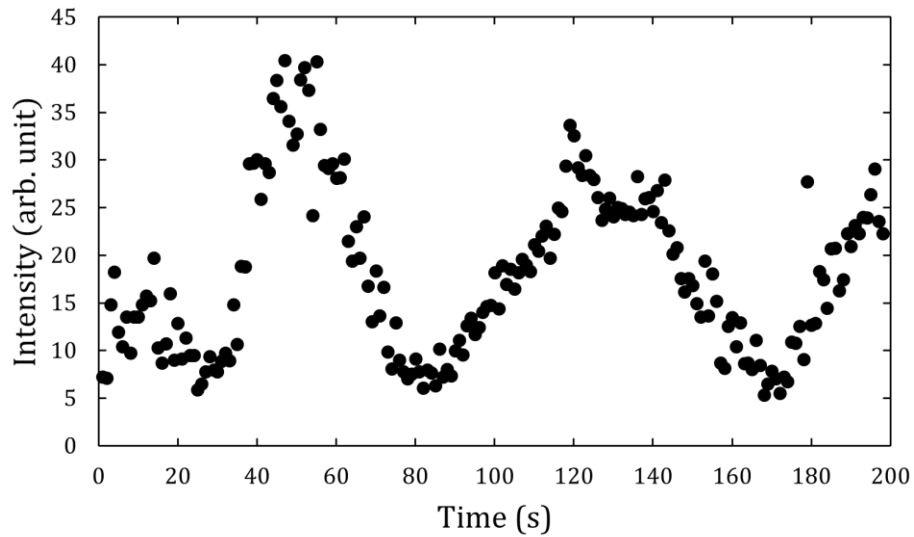


Figure 23. Image of a graph showing the intensity of a pixel over time from last year. The graph does not look like a sine function like it should. This means that the mirror was not moving at a constant speed.

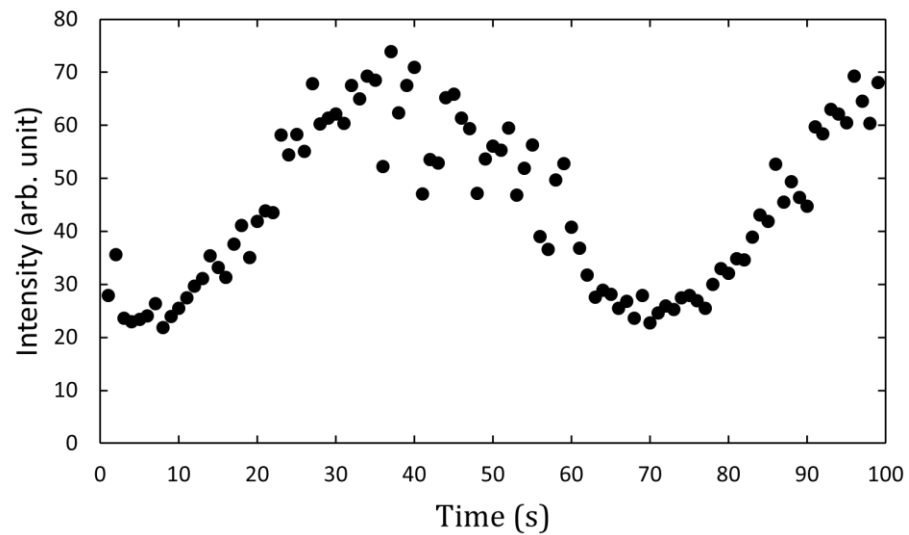


Figure 24. Plot of a graph showing the intensity of a pixel over time from this year. The plot can be fitted using a sine function.

The topography of the mirror can be seen in Figure 25. Looking at this image, a dome like shape appears to exist on the mirror. This dome shape comes from a slight misalignment of the collimating lenses that are used in the apparatus.

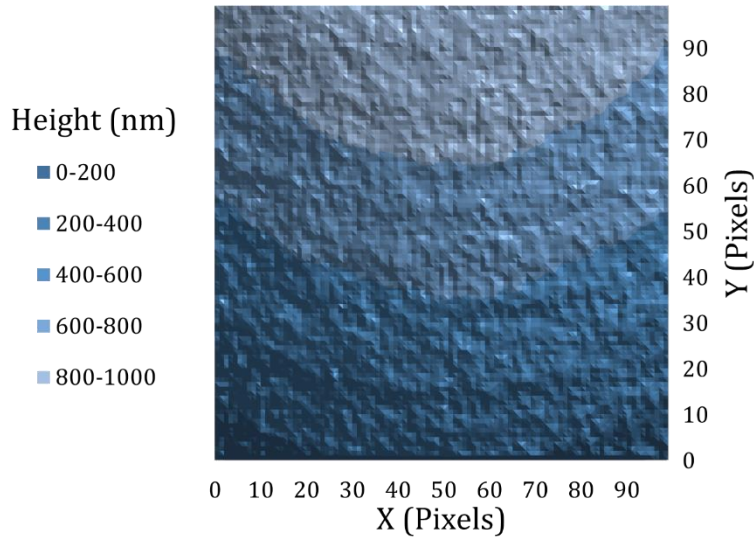


Figure 25. Surface topography of the section of the mirror outlined in Figure 22. The topography increases towards the top of the section of the mirror. This topography shows a dome like shape in the mirror. This dome is from the different lenses not being aligned. Each pixel is roughly 0.044 mm^2 of the sample.

4.2. *Determining Timing of Tests*

To determine how long each test should be, multiple tests were done using different time periods for the voltage on the reference mirror to scan from 0 to 5 V. Figure 24 shows a test from this year that was 100 s long. Figure 26 shows a test that was 50 s long, and Figure 27 shows a test that was 200 s long. The fit of the graphs in the test that was 200 s long, and 50 s long, is not as good as the one with 100 s long. This shows that with the current setup, the best way of running the test is running it for 100 s. These tests shown in Figure 26 and Figure 27 were done at night on a weekend. This was to limit the number of people that would be in the building at the time of testing. These tests were also done within 20 min of each other.

Another problem involving timing that needed to be solved is what time of day the tests needed to be done. The test from Figure 24 was done at night when less people were in the building. At this time, it was much less likely that someone was to be walking around, causing

the apparatus to vibrate and not function correctly. Figure 28 shows a test that was done during the day. The data from this test is not accurate at all and cannot be used to get the topography of the mirror.

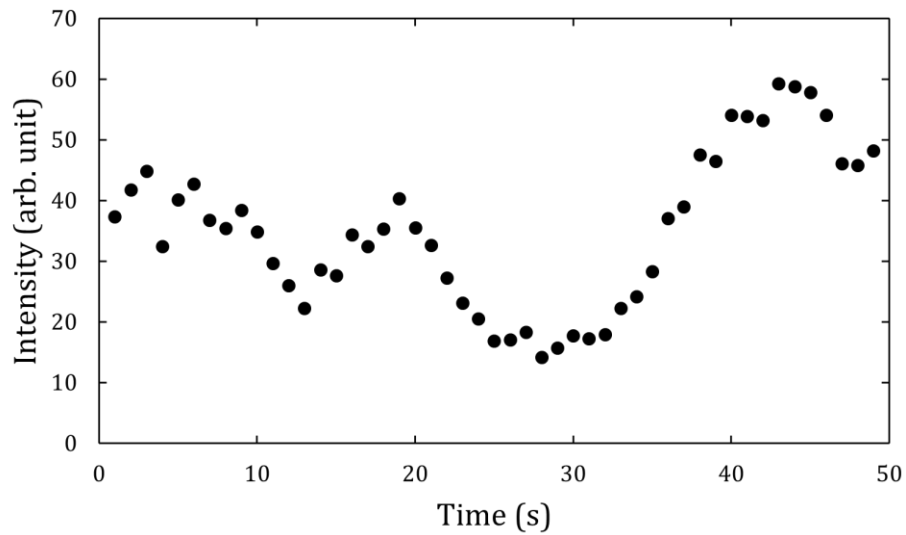


Figure 26. Plot of a test done that was 50 s long, with 50 total pictures. The test does not fit a sine function well, showing that moving the mirror too fast can cause the data to not be accurate.

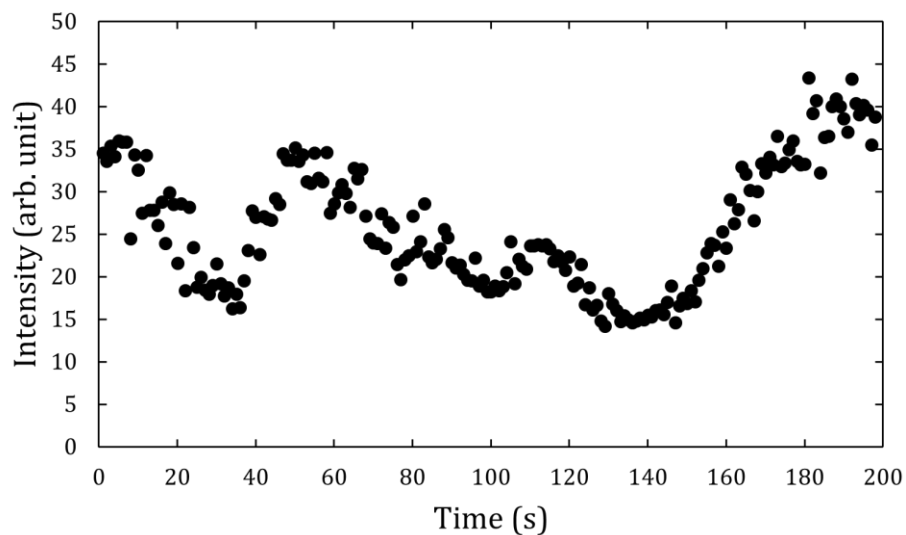


Figure 27. Plot of a test done that was 200 s long, with 200 total pictures. The plot does not fit a sine function well, and there is a lot of noise. This shows that moving the mirror too slow can cause the data to be inaccurate.

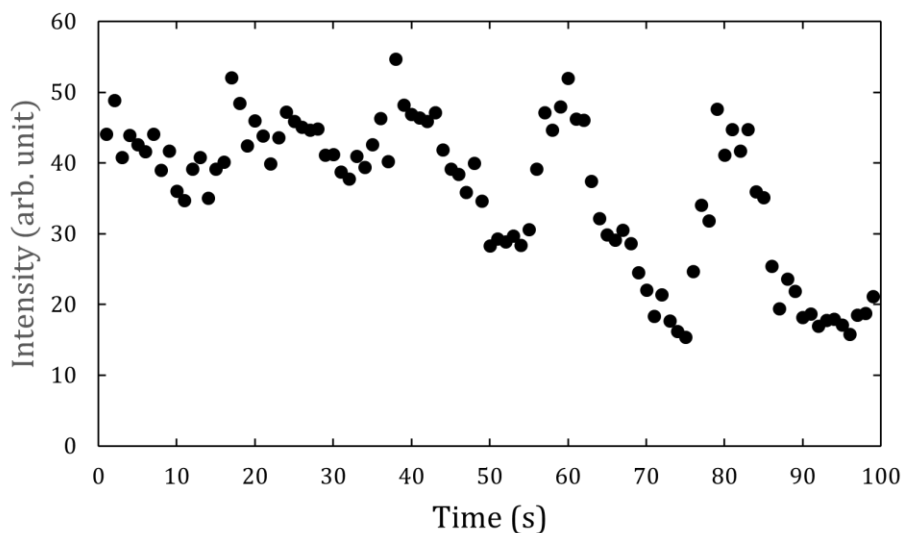


Figure 28. Plot of a test done during the day. The poor sine function fit shows that taking data during the daytime introduces too much noise.

4.3. *Repeatability*

After the machine was operational, multiple tests were done to determine how well the apparatus was working. Figure 29 shows two tests that were done on the same test surface in quick succession of each other. This was done to limit the number of outside factors that can change the image. This can include someone bumping into the machine, or anything moving due to vibrations. An intensity plot of the difference between the two tests can be seen in Figure 30. The standard deviation of the difference between two corresponding values is 3.9 nm and the mean is -1.8 nm.

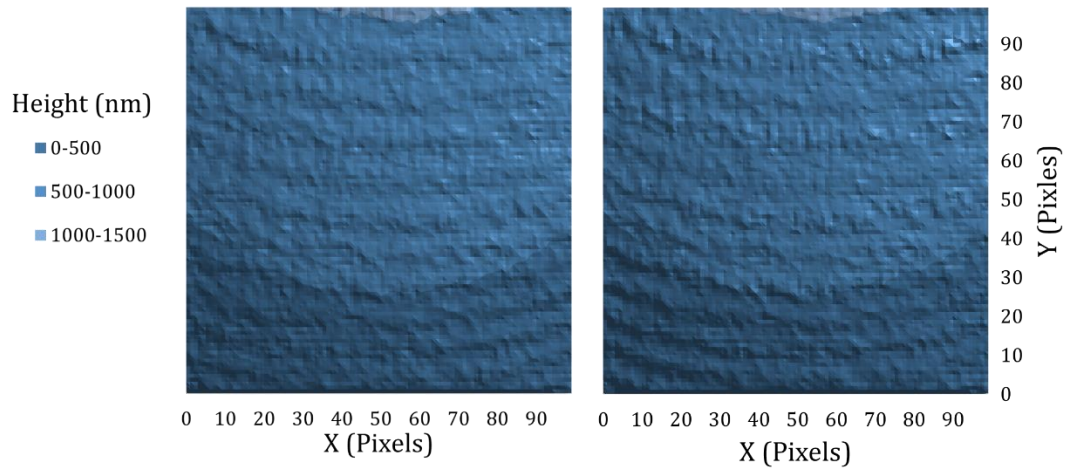


Figure 29. Surface topography of tests done in quick succession of each other. The similarity of these tests, as well as the low standard deviation of the differences shows that it is possible to get repeated results using this apparatus. Each pixel is roughly 0.044 mm^2 of the sample.

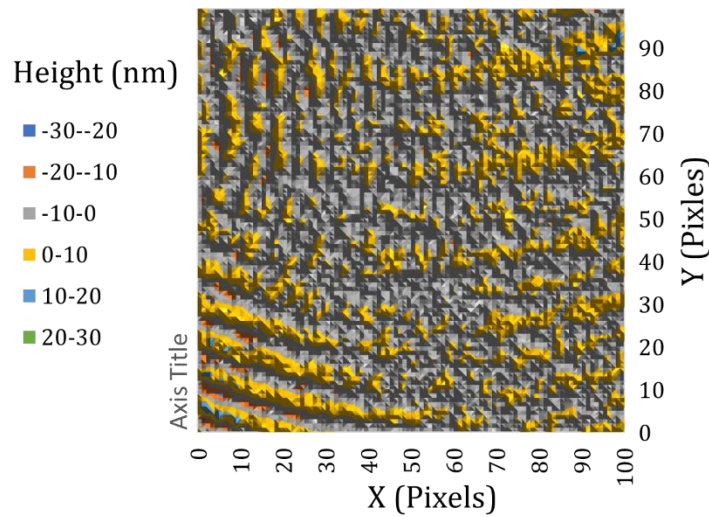


Figure 30. Plot of the difference between the two tests shown in Figure 29. The standard deviation of the differences is 3.9 nm and the mean is -1.8 nm. This shows that tests can be repeated. Each pixel is roughly 0.044 mm^2 of the sample.

Chapter 5

CONCLUSION/FUTURE PLANS

Now that all the mechanical parts of the interferometer have been tested, it is time to focus on the electronics side of the interferometer. The next step of the interferometer is to switch the programming language that is being used for the different aspects of the interferometer. These include moving the reference mirror, data analysis, and taking pictures of the interference pattern. The current programming language that is being used to move the reference mirror and perform the data analysis is LabVIEW. The pictures of the interference pattern are currently taken using Yawcam. The new programming language that is being used is Processing, which is what the Arduino programming language is based on. Using this programming language gives the ability to use a camera using the program, making it easier to collect data. This programming language also allows the interferometer to be used from a more remote position.

Future testing of the interferometer will also be done using actual thin films that have been produced on 10 cm diameter Si substrates. Two of these films have been made, and a plan to produce more is currently in the works. The films that will be produced in the future will have an uncoated stripe down the middle of the substrate and produce a gradient thickness from 0 nm to some maximum thickness. It will then be possible to determine the thickness of the thin metal film by comparing the topography of the stripe to that of the portion of the film alongside the stripe.

References

-
- [1] T. Young, Philosophical Transactions of the Royal Society of London **94**, 1 (1804).
 - [2] E.H. Cook, The London, Edinburgh, and Dublin Philosophical Magazine and Journal of Science **7**, 225 (1879).
 - [3] A.A. Michelson, American Journal of Science **s3-22**, 120 (1881).
 - [4] F. Twyman and A. Green, U. S. Patent No. 1,252,512 (8 January 1918).
 - [5] R.P. Grosso and R. Crane, Jr., in Proceedings of the 23rd Annual Technical Symposium, San Diego, United States, 1979.
 - [6] C.-L. Tien, Y.-R. Lyu, and S.-S. Jyu, Applied Surface Science **254**, 4762 (2008).
 - [7] F. Twyman, The London, Edinburgh, and Dublin Philosophical Magazine and Journal of Science **35**, 49 (1918).
 - [8] F. Twyman, Transactions of the Optical Society **22**, 174 (1921).
 - [9] D.K. Sharma and J. Schwider, in *Proceedings of the International Conference on Optics and Optoelectronics, Dehradun, India, 1999*.
 - [10] J.S. Darlin, M.P. Kothiyal, and R.S. Sirohi, Journal of Modern Optics **45**, 2371 (1998).
 - [11] J.B. Houston, C.J. Buccini, and P.K. O'Neill, Applied Optics **6**, 1237 (1967).
 - [12] L.J. Steimle and Y. Wang, in *Proceedings on Infrared Spaceborne Remote Sensing, San Diego, United States, 1993*.
 - [13] T.H. Maiman, R.H. Hoskins, I.J. D'Haenens, C.K. Asawa, and V. Evtuhov, Physical Review **123**, 1151 (1961).
 - [14] W.M. Farmer, Applied Optics **13**, 610 (1974).
 - [15] M. Skalsky, J. Fialka, and Z. Havranek, in *Proceedings of the IEEE International Instrumentation and Measurement Technology Conference, Auckland, New Zealand, 2019*, p. 1-6.
 - [16] A.J. van Haasteren and H.J. Frankena, Applied Optics **33**, 4137 (1994).
 - [17] D.W. Robinson and D.C. Williams, Optics Communications **57**, 26 (1986).
 - [18] M. Schwertner, M.J. Booth, M.A. Neil, and T. Wilson, Journal of Microscopy **213**, 11 (2004).
 - [19] I.V. Antonets, L.N. Kotov, S.V. Nekipelov, and E.N. Karpushov, Technical Physics **49**, 1496 (2004).
 - [20] C.-L. Tien, H.-M. Yang, and M.-C. Liu, Thin Solid Films **517**, 5110 (2009).
 - [21] S.-W. Kim and G.-H. Kim, Applied Optics **38**, 5968 (1999).
 - [22] Y.-S. Ghim and S.-W. Kim, Applied Optics **48**, 799 (2009).
 - [23] J. Malone, B.S. thesis, Houghton University, 2021.
 - [24] S. Olandt, B.S. thesis, Houghton University, 2019.